SP-230—51

Flexural Behavior of Fiber-Reinforced-Concrete Beams Reinforced with FRP Rebars

by H. Wang and A. Belarbi

Synopsis: The main objective of this study was to develop a nonferrous hybrid reinforcement system for concrete bridge decks by using continuous fiber-reinforced-polymer (FRP) rebars and discrete randomly distributed polypropylene fibers. This hybrid system has the potential to eliminate problems related to corrosion of steel reinforcement while providing requisite strength, stiffness, and desired ductility, which are shortcomings of the FRP reinforcement system in reinforced concrete structures.

The overall study plan includes (1) development of design procedures for an FRP/FRC hybrid reinforced bridge deck system; (2) laboratory studies of static and fatigue bond performances and ductility characteristics of the system; (3) accelerated durability tests of the hybrid system; and (4) static and fatigue tests on full-scale hybrid reinforced composite bridge decks. This paper presents the results relating to the flexural behavior of the polypropylene-fiber-reinforced-concrete beams reinforced with FRP rebars.

Test results indicated that with the addition of fibers, the flexural behavior was improved with an increase of ductility index by approximately 40% as compared to the plain concrete beams. Crack widths of FRP/FRC were found to be smaller than those of FRP/plain concrete system and the values predicted by the current ACI 440 equations. Furthermore, the compressive failure strains of concrete in FRP/FRC beams exceed the strain of 0.0040 mm/mm.

Keywords: concrete bridge decks; crack width; ductility; fiber-reinforced concrete; fiber-reinforced polymers; flexure; polypropylene fiber

Huanzi Wang, Ph.D.**,** is an assistant engineer at Biggs Cardosa Associates, Inc, California. He received his Ph.D. degree in Civil Engineering at the University of Missouri – Rolla. He received his BS and MS in structural engineering from the Southeast University, China. His research interest includes the application of FRP reinforcement to the concrete structure design. He is a member of ACI.

Abdeldjelil Belarbi, FACI, is a Distinguished Professor at the University of Missouri - Rolla. His research interests include constitutive modeling of reinforced and prestressed concrete as well as use of advanced materials and smart sensors in civil engineering infrastructure. He is a member of joint ACI-ASCE committees 445, and ACI Committees 440. He is Chair of subcommittee 445-5 (Torsion) and past Chair of E801.

INTRODUCTION

Ductility is a structural design requirement in most design codes. In steel RC structures, ductility is defined as the ratio of post yield deformation to yield deformation which it usually comes from steel. Due to the linear-strain-stress relationship of FRP bars, the traditional definition of ductility cannot be applied to structures reinforced with FRP reinforcement. Several methods, such as the energy based method and the deformation based method, have been proposed to calculate the ductility index for FRP reinforced structures.[1-2]

Due to the linear elastic behavior of FRP bars, the flexural behavior of FRP reinforced beams exhibits no ductility as defined in the steel reinforced structures. A great deal of effort has been made to improve and define the ductility of beams reinforced with FRP rebars. To date, there are two approaches; one approach is to use the hybrid FRP rebars; that is, pseudo-ductile materials are fabricated by combining two or more different FRP reinforcing materials to simulate the elastic-plastic behavior of the steel rebars. Belarbi, Chandrashekhara and Watkins[3] and Harris, Somboonsong, and Ko[4] tested beams reinforced with the hybrid FRP reinforcing bars and they found that the ductility index of those beams could be close to that of the beams reinforced with steel. This method has shown some success in the research studies but has resulted in limited practical applications because of the complicated and costly manufacturing process of the hybrid rebars. The other approach is to improve the property of concrete. ACI 440[5] recommends the FRP reinforced structures be over-reinforced and designed so that the beams fail by concrete crushing rather than by rebar rupture. Thus, the ductility of the system is strongly dependent on the concrete properties. Alsayed and Alhozaimy[6] found that with the addition of 1% steel fibers, the ductility index can be increased by as much as 100%. Li and Wang[7] reported that the GFRP rebars reinforced with engineered cementitious composite material showed much better flexural behaviors. The ductility was also found to be significantly improved.

This paper presents research result on the flexural behavior of concrete beams reinforced with FRP rebars and concrete containing polypropylene fibers. The different behaviors of plain concrete beams and FRC beams are also discussed.

EXPERIMENTAL PROGRAM

A total of 12 beams making 6 testing groups were investigated. Each testing group was composed of two similar beams, one subjected to monotonic loading and the other subjected to repeated loading/unloading. The experimental variables included FRP rebar size (#4 vs. #8), rebar type (GFRP vs. CFRP), and plain concrete vs. FRC.

Materials

FRP Rods--three types of commonly used FRP rods were adopted in this study: namely the #8 (25mm) glass fiber reinforced polymer (GFRP), #4 (13 mm) GFRP, and #4 (13mm) carbon fiber reinforced polymer (CFRP), as shown in Fig. 1. The surface of the GFRP rods is tightly wrapped with a helical fiber strand to create indentations along the rebar, and sand particles are added to the surface to enhance its bonding strength. For the #4 GFRP, the pitch of the fiber strand is about 25.4 mm and helically rounded about 60 degrees to the longitudinal direction. For the #8 GFRP, the pitch of the fiber strand is 22 mm and helically rounded about 75 degrees to the longitudinal direction. The surface of the CFRP is very smooth, as shown in Fig. 1. The resin used for these bars is epoxy modified vinyl-ester for both GFRP rebar and CFRP rebar. Based on the information provided by the manufacturer, the ultimate tensile strengths for #4 GFRP, #8 GFRP and #4 CFRP are 690 MPa, 552 MPa, and 2,069 MPa, respectively. The elastic moduli are 41 GPa, 41 GPa, and 124 GPa, respectively.

Polypropylene Fibers--currently, many fiber types are commercially available including steel, glass, synthetic, and natural fibers. To fulfill the total steel-free concept, polypropylene fiber was used in this study. The fibers were fibrillated and commercially available in 57 mm length.

Concrete--the concrete mix used in this study was based on an existing MoDOT mix design. For practical application, the volume fraction (V_f) of 0.5% of polypropylene fibers was used to make the FRC and take the benefits of the fibers, while ensuring good workability of concrete. It should be noted that the purpose of this study was to qualitatively investigate the benefits gained from the fibers to the FRP reinforcing system The different volume fraction's effect was not a variable to be investigated in this study. The compression strength of concrete on the day of testing was 30 MPa and 48 MPa for FRC and plain concrete, respectively.

Test Specimens

The beams were 178 mm wide, 229 mm high, and 2032 mm long. To avoid shear failure, traditional #3 steel U-shape stirrups with a spacing of 89 mm were used as shear reinforcement at both ends of the beams. To minimize the confining effect of the shear reinforcement on the flexural behaviors, no stirrups were used in the testing regions (pure bending regions). A concrete clear cover of 38 mm was used for all beams. All beams were designed to fail by concrete crushing, as recommended by the current ACI 440. This was accomplished by using a reinforcement ratio greater than the balanced reinforcement ratio ρ_b.

The notation for the specimen's identification is as follows: the first character, "P" or "F", indicates plain concrete or FRC; the second character, "4" or "8", indicate the rebar size in English designation used as reinforcement; the last character, "C" or "G", indicates the rebar type, CFRP or GFRP. Details of the specimens are shown in Table 1.

Test Setup and Procedures

Beams were subjected to a four-point flexural testing, as shown in Fig. 2. Beams were instrumented with three LVDTs in the testing region (pure bending region) to monitor the mid-span deflection and determine the curvature. FRP rebars were instrumented with strain gauges to measure rebar deformation. Two LVDTs were mounted at the top surface of the beam to record the compressive concrete strain. In the testing region, Demac gages were bonded to the beam surface, 38 mm above the bottom (the same level as the longitudinal rebars) to measure the crack widths. A microscope was also used to measure the crack width at the rebar location. Another two LVDTs were mounted at the ends of the beam to record the relative slips between the longitudinal rebar and the concrete (the longitudinal rebars were protruded about 10 mm from the ends). Load was applied in increments by a hydraulic jack and measured with a load cell. Three increments were taken up to the initiation of cracking and ten increments up to failure. At the end of each load increment, the load was held constant, crack patterns were photographed, and near mid-span crack widths were recorded.

Each testing parameter was investigated using two identical specimens, as shown in Table 1. One beam was loaded monotonically to failure. The other beam was subjected to repeated loading/unloading cycles at 40% and 80% of its capacity to evaluate the residual deflection, residual crack width, as well as the energy absorption capacity.

TEST RESULTS AND DISCUSSIONS

This section will provide a summary of the overall flexural behaviors of the FRP/FRC hybrid system in terms of crack distribution, load-deflection response, relative slip between the rebar and concrete, cyclic loading effect on flexural behavior, and strain distribution in concrete and reinforcement. Comparison between FRP/Plain concrete system and FRP/FRC system is also discussed.

Crack Spacing

Table 2 shows the average crack spacing at 40% and 80% of the flexural capacity. With the increase of load, crack spacing slightly decreased. Interestingly, by comparing the crack spacing between the plain concrete beams and the FRC beams, the crack spacing was virtually the same at 80% of ultimate load for both plain concrete and FRC beams, while the crack spacing of the FRC beams was about 20% smaller than that of plain concrete beams at service load (40% of ultimate load).

Studies suggest that the flexural cracking can be closely approximated by the behavior of a concrete prism surrounding the main reinforcement and having the same centroid. Cracks initiate when the tensile stress in the concrete exceeds the tensile strength of concrete, f_t'. When this occurs, the force in the prism is transferred to the

rebar. Away from the crack, the concrete stress is gradually built up through the bond stress between the rebar and the concrete. When the stresses in the concrete are large enough and exceed the tensile strength of concrete f_t', a new crack forms. The above mechanism is demonstrated in Fig. 3(a).

With the addition of fibers, the mechanism of crack formation is slightly changed, as shown in Fig. 3(b). Some tensile loads can be transferred across the cracks by the bridging of fibers. Thereby, the stress in the concrete comes from not only the bond stress but the bridging of fibers as well. With the contribution from the fibers, less bond stress is needed to reach the same cracking stress. Consequently, the spacing of crack is smaller in the FRC beams than in the plain concrete beams ($S_2 < S_1$ as shown in Fig. 3).

At the high level of load, due to loss of bond between the fibers and concrete, fibers are pulled out and the contribution from the bridging of fibers is diminished.

Crack Width

During the tests, crack widths were measured by the Demac gages. Fig. 4 through 6 show the relationships between the crack width and the applied moment. In the following section, several currently available models to predict the crack width are discussed and compared with test results.

Based on the well-known Gergely-Lutz[8] equation, the current ACI 440 recommends a similar equation to calculate the crack width of the FRP reinforced member as follows:

$$w = \frac{2200}{E_f} k_b \beta f_f \sqrt[3]{d_c A} \tag{1}$$

where w is the crack width at tensile face of the beam,

A is the effective tension area per bar,

d_c is the thickness of concrete cover measured from extreme tension fiber to the center of the closest layer of longitudinal bars,

f_f is the stress in the FRP reinforcement,

β is the coefficient to converse crack width corresponding to the level of reinforcement to the tensile face of beam, and

k_b is the coefficient that accounts for the degree of bond between the FRP bar and the surrounding concrete. ACI 440 does not give a mathematical relationship between k_b and the bond strength. It suggests a value of 1.2 for deformed FRP bars if k_b is not experimentally known.

Toutanji and Saafi[8] reported that the crack width is a function of the reinforcement ratio. They proposed the following equation to predict the crack width:

$$w = \frac{200}{E_f \sqrt{\rho_f}} \beta f_f \sqrt[3]{d_c A} \tag{2}$$

where ρ_f is the reinforcing ratio.

Based on the equivalent beam concept, Salib and Abdel-Sayed[10] proposed the following equation:

$$w = 0.076 \times 10^{-3} \times \{(E_s / E_f)(u_{b,s} / u_{b,f})^{2/3}\} \times \beta f_f \sqrt[3]{d_c A} \quad (3)$$

By substituting E_s=29000 ksi, Equation 3 becomes

$$w = \left(\frac{2200}{E_f} \times \sqrt[(2/3)]{\frac{u_{b,s}}{u_{b,f}}} \right) \times \beta f_f \sqrt[3]{d_c A} \quad (4)$$

where $u_{b,f}$ and $u_{b,f}$ are the bond strengths of steel rebar and FRP rebar, respectively.

In Equation 4, the values of $u_{b,f}$ and $u_{b,f}$ need to be evaluated and decided upon. For traditional steel rebar, according to ACI 318-02,[11] $l_d = \frac{f_y d_b}{25\sqrt{f_c'}}$ (neglecting the adjusting coefficients) and based on the definition of the development length,

$$\pi d_b l_d u_{b,s} = f_y A_s = f_y (\pi d_b^2) / 4 \quad (5)$$

one gets: $u_{b,s} = 6.25\sqrt{f_c'}$.

For FRP rebar used in this study, based on the previous bond study (Belarbi and Wang[12]), $u_{b,f} = 9.25\sqrt{f_c'}$. Based on this approximate values of u_b $u_{b,f}$ and $u_{b,f}$, Equation 4 become

$$w = \frac{1700}{E_f} \beta f_f \sqrt[3]{d_c A} \quad (6)$$

All the above equations were developed based on the Gergely-Lutz model. However, different researchers proposed different models to account for the bond strength effect and/or reinforcement ratio effect on the crack width.

As shown in Figs. 4 through 6, the Salib *et al.* model gives reasonable predictions of the crack width for both plain concrete beams and FRC beams. For the Toutanji *et al.* model, the prediction values show poor correlation with the experimental results. When for low reinforcing ratios, (for the CFRP beams, ρ=0.67%), the model overestimates the crack width. Vice versa, for high reinforcing ratios (#4 GFRP beams, ρ=2.2%, and #8 GFRP beams, ρ=3.3%), the model underestimates the crack width. Therefore, it may be concluded that it is the bond characteristics rather than the reinforcing ratio that affect the crack width.

The predictions based on current ACI 440 equations were also compared with the test results. The accuracy of the equation largely depends on the value of k_b. Even when selecting k_b =1.0, one can see that the predictions are still conservative.

Fiber Effect on Crack Width-

With the addition of fibers, the crack widths were slightly decreased at the same load level, especially at the service load, as shown in Fig. 4 through 6.

As shown in Table 3, the crack widths were smaller in the case of FRC beams as compared to plain concrete beams at the service load. As discussed earlier, the crack spacing was decreased at the service load due to the contribution from the fibers. Since

the crack width is proportionally related to the crack spacing, the crack width is expected to be smaller in the FRC beams at service loads.

Load-Deflection Response

Figs. 7 through 9 show the typical experimental moment-deflection curves for plain concrete beams and FRC beams reinforced with different types of FRP rebars. With the increasing of moment, cracks occurred in the testing region when the moment exceeded the cracking moment M_{cr}. Consequently, the flexural stiffness of the beams was significantly reduced and the curves were greatly softened. As expected, due to the linear-elastic behavior of the FRP rebars, the FRP reinforced beams showed no yielding. The curves went up almost linearly until the crushing of concrete.

Fiber Effect on Moment-Deflection Curves

In order to compare the flexural behaviors between plain concrete beams and FRC beams, all the load-deflection curves of the plain concrete beams were normalized, based on the following rules: 1) moment was divided by a coefficient C_M, defined as $C_M = \frac{M_{ACI-plain}}{M_{ACI-FRC}}$, where $M_{ACI\text{-}plain}$ and $M_{ACI\text{-}FRC}$ are theoretical ultimate capacities computed based on ACI 440 for beams with concrete strengths equal to the plain concrete beams and the FRC beams, respectively; 2) deflection was divided by a coefficient C_D, defined as $C_D = \frac{\Delta_{ACI-plain}}{\Delta_{ACI-FRC}}$, where $\Delta_{ACI\text{-}plain}$ and $\Delta_{ACI\text{-}FRC}$ are theoretical deflection based on ACI 440 for beam with concrete strengths equal to the plain concrete beams and FRC beams at the service load (40% of the ultimate load), respectively.

As shown in Table 4 and Figs. 7 through 9, with the addition of fibers, the ultimate moments and deflections were increased. The plain concrete beams failed in a more brittle and explosive manner. Once it reached the capacity, the concrete was crushed and the load dropped suddenly and violently. FRC beams failed in a more ductile way as the load dropped more gently and smoothly.

Theoretical Correlation

Deflection at mid-span for a simply supported beam of total length L and subjected to a four-point flexural test is given as

$$\Delta_{mid} = \frac{Pa}{24E_cI_e}(3L^2 - 4a^2) + \frac{Ph^2a}{10GI_e} \tag{7}$$

The first term on the right is from the flexural component, and the second term is from the shear component. In this study, testing beams had a span-depth ratio of 2.67. Based on calculation, it was found that the shear component was about 3% of the flexural component. It was, therefore, neglected for simplicity. Thus, Equation 7 becomes

$$\Delta_{mid} = \frac{Pa}{24E_cI_e}(3L^2 - 4a^2) \tag{8}$$

Current ACI 440 recommends the following expressions to calculate the effective moment of inertia I_e:

$I_e = I_g$ when $M_a \le M_{cr}$;

$$I_e = \left(\frac{M_{cr}}{M_a}\right)^3 \beta_d I_g + \left[1 - \left(\frac{M_{cr}}{M_a}\right)^3\right] I_{cr} \le I_g \text{ when } M_a > M_{cr} \quad (9)$$

where $\beta_d = \alpha_b \left[\frac{E_f}{E_s} + 1\right]$, and ACI 440 recommends taking the value of $\alpha_b = 0.5$ for all the FRP bar type. (10)

As shown in Figs. 7 through 9, ACI 440 equations predict the moment-deflection response fairly well, especially at the service stage. Thus, the equations recommended by the current ACI 440 would be used for design purpose for both plain concrete beams and FRC beams.

Relative Slip between Longitudinal Rebar and Concrete at Beam Ends

No relative slips were observed in any of the test beams. That means that the development lengths as designed by the previous bond study (Belarbi and Wang[12]) were adequate for the FRP bars to develop the required forces.

Loading/Unloading Effect on the Flexural Behaviors

No significant differences were observed before and after loading and unloading cycles in the crack width, crack distribution, and deflection. Also, the flexural stiffness did not change after cyclic loading, as shown in Figs. 10 and 11.

Strains in Reinforcement and Concrete

Fig. 12 presents the typical measured mid-span strains in reinforcement and in concrete versus the applied moment. It can be seen that after cracking, the strains in the reinforcement increased almost linearly up to failure. Because all test beams failed in concrete crushing rather than FRP reinforcement rupture, all the maximum measured strains in the reinforcement were less than the ultimate tensile strains. In beams reinforced with #4 CFRP, #4 GFRP, and #8 GFRP, the maximum measured strains were 12,000, 12,000, and 8,000 microstrains, respectively; while the ultimate strains were 16,700, 16,900, and 13,500 microstrains, respectively.

The differences of the moment-strain curves between the plain concrete beams and the FRC beams are significant. In plain concrete beams, once reaching the ultimate, concrete failed by crushing, and strains in the reinforcement dropped suddenly. However, in FRC beams, when beams reached the ultimate, concrete was held together and the strains in concrete and strains in reinforcement kept increasing gradually. Furthermore, with the addition of fibers, the ultimate strain for the concrete was increased. In plain concrete beams, the measured ultimate concrete strains ranged from 2,700 microstrains to 3,300 microstrains with an average of 2,950 microstrains. In FRC beams, the measured ultimate concrete strains ranged from 4,000 microstrains to 5,500 microstrains with an average of 4,500 microstrains.

It should be noted that with the increase of ultimate concrete strain, the balanced reinforcing ratio, ρ_{bf}, will increase accordingly. Herein, ρ_{bf} is defined as follows

$$\rho_{bf} = 0.85\beta_1 \frac{f_c'}{f_{fu}} \frac{\varepsilon_{cu}}{\varepsilon_{cu} + \varepsilon_{fu}} \tag{11}$$

From this standpoint, in order to take advantage of FRC, more reinforcements are required to achieve failure by crushing of concrete. This results in additional gain of moment capacity.

PREDICTIONS OF THE ULTIMATE FLEXURAL CAPACITY

As shown in Table 1, the reinforcing ratio, ρ_f, for all the beams were taken greater than the balanced ratio, ρ_{bf}, where ε_{cu}=0.003 as defined by ACI 318-02.[11] As expected, all beams failed in concrete crushing.

Predictions by the ACI 440 equations were based on the normal assumptions of the flexural theory of concrete reinforced beams. The governing equations are as follows:

$$M_n = \rho_f f_f \left(1 - 0.59 \frac{\rho_f f_f}{f_c'}\right) bd^2 \tag{12}$$

$$f_f = \left(\sqrt{\frac{(E_f \varepsilon_{cu})^2}{4} + \frac{0.85\beta_1 f_c'}{\rho_f} E_f \varepsilon_{cu}} - 0.5 E_f \varepsilon_{cu} \right) \le f_{fu} \tag{13}$$

There are two possible ways by which fibers can increase the flexural strength: one is that the fibers function as auxiliary reinforcement to carry some tensile stresses; the other way is that the fibers can improve the concrete properties. In this study, contribution of fibers in tensile strength was neglected since

(1) Compared to the steel fibers, the tensile strength of polypropylene fibers is low: less than 1/3 of the tensile strength of the steel fibers.
(2) Due to the low elastic modulus of polypropylene fiber (500 to 700 ksi), the elongation at break is three orders of magnitude greater than the tensile strain at failure of the concrete. Hence, the concrete will crack long before the fiber strength is approached.

Thus, the most likely contribution from the fibers to increase the flexural strength is to improve the concrete properties. In this study, as described earlier, the ultimate concrete strain, ε_{cu}, was found to be large than 0.003 in the presence of fibers in the order of 0.0045 mm/mm.

As shown in Table 5, the theoretical predictions agreed well with the test results. As discussed earlier, the concrete strains of the FRC beams at failure were greater than 0.0035 on average. For the design of the FRC beams, if we could assume ε_{cu} to be equal to 0.0035, with is slightly larger than the assumed value of 0.003 of plain concrete.

DUCTILITY

As mentioned previously, since the traditional definition of ductility can not be applied to the structures reinforced with FRP reinforcement, there was a need for developing a new approach and a set of ductility indices to both quantitatively and qualitatively evaluate the FRP reinforced members.

Ductility index calculations related to the FRP reinforced members have been widely studied. Two approaches have been in the literature proposed to address this problem.

Energy Based Approach

Based on the definition of the energy based approach, ductility can be defined as the ratio between the elastic energy and the total energy, as shown in Fig. 13.

Naaman and Jeong[1] proposed the following equation to compute the ductility index, μ_E:

$$\mu_E = \frac{1}{2}\left(\frac{E_t}{E_e} + 1\right) \tag{14}$$

where E_t is the total energy computed as the area under the load deflection curve; and E_e is the elastic energy. The elastic energy can be computed as the area of the triangle formed at failure load by the line having the weighted average slope of the two initial straight lines of the load deflection curve, as shown in Fig. 13.

Deformation Based Approach

The deformation based approach was first introduced by Jaeger, Tadros, and Mufti.[2] It takes into account the strength effect as well as the deflection (or curvature) effect on the ductility. Both the strength factor and the deflection (or curvature) factor are defined as the ratio of moment or deflection (or curvature) values at ultimate to the values corresponding to the concrete compressive strain of 0.001. The strain of 0.001 is considered the beginning of inelastic deformation of concrete.

$$Deformability\ factor = strength\ factor \times deformability\ factor\ (deflection\ or\ curvature)\ factor$$

$$Strength\ factor = \frac{moment\ at\ ultimate}{moment\ at\ concrete\ strain\ of\ 0.001}$$

$$Deflection\ factor = \frac{deflection\ at\ ultimate}{deflection\ at\ concrete\ strain\ of\ 0.001}$$

$$Curvature\ factor = \frac{curvature\ at\ ultimate}{curvature\ at\ concrete\ strain\ of\ 0.001}$$

In the following sections, ductility indices based on both approaches are computed and compared.

Ductility Index Computed by the Energy Based Method

As shown in Fig. 12, the definition of elastic slope is dependent on the selections of P1, P2, S1, and S2. Also, the experimental moment-deflection curves, as shown in Figs. 7

through 9, were difficult to be idealized into three portions with three distinct slopes and it could induce some subjective errors if the curves were artificially divided. In this study the elastic slopes were decided by the slopes of loading/unloading cycles during the tests rather than using the theoretical predictions proposed by Naaman and Jerong.[1] The ductility indices computed are shown in Table 6.

Ductility Index Computed by the Deformation Based Method

Theriault, Benmokrane, and Gao[13] found that the ductility indices computed by the curvature factor demonstrated more consistent comparison to those computed by deflection factor. Therefore, the curvature factor is adopted in this study. The ductility indices are computed as shown in Table 7.

Discussions of Ductility Index

As shown in Tables 6 and 7, the ductility indices computed by the two methods are quite different. Ductility indices by the Naaman and Jerong method are much smaller than those by the Jaeger method. Another significant difference is that the effect from the addition of fibers on the ductility indices is much more pronounced when calculated based on the Jaeger method.

A schematic load-deflection curve for a certain material reinforced beam, as shown in Fig. 14, is created to explain the different results by the two methods. With the addition of fibers, the load capacity and deflection are increased from P1 to P2 and $\Delta 1$ to $\Delta 2$, proportionally.

Although there are different ways to calculate the ductility index, ductility can no doubt be defined as the ability to absorb the inelastic energy without losing its load capacity. Higher inelastic energy absorption of the same system means higher ductility. Obviously, from this standpoint, the addition of fibers significantly improves the system's ductility. However, based on the prediction of Naaman and Jerong's ductility index, the ductility is the same before and after the addition of fibers. Because the ratios of $\frac{E_t}{E_e}$ are the same, μ_E does not change. The reason is although the absorption of the inelastic energy with the addition of fibers increases, the absorption of the elastic energy is also increased proportionally. Thus, the index μ_E remains constant in this example. From this standpoint, the ductility index proposed by Naaman and Jerong cannot efficiently take into account the benefits gained from the increase of the ultimate moment capacity and the accompanying increase of the deflection with the addition of fibers. The ductility index based on the Jaeger approach is more reasonable. It not only considers factors resulting from the load capacity, but it also considers the deformation effect on the ductility. The ductility increases approximately 40% with the addition of fibers, based on the Jaeger approach. Also, all the ductility indices, as calculated by the Jaeger method, were found to be above the lower limit of 4 recommended by Jaeger and the Canadian Highway Bridge Design Code.[14] Both the plain concrete beams and the FRC beams can, therefore, be considered acceptable for design in terms of ductility requirement.

CONCLUSIONS

An extensive research program was initiated to investigate the feasibility of steel-free hybrid reinforcement system for concrete bridge decks by combining FRP reinforcement with the polypropylene fiber reinforced concrete. From the flexural study covered in this paper, the following conclusions can be drawn:

1. The deflection predicted by the current ACI 440 matches the experimental results fairly well, especially at the service load, and it is suggested to be used for the design purpose for both the plain concrete beams and the FRC beams.
2. The model proposed by Salib *et al*. gives reasonable predictions of the crack width for both plain concrete beams and FRC beams. The predictions by the ACI 440 are conservative.
3. With the addition of fibers, the crack widths are smaller at service load in the case of FRC beams as compared to plain concrete beams.
4. The concrete ultimate strains measured in FRC beams were larger than that of the plain concrete beams. They ranged from 4,000 microstrains to 5,500 microstrains with an average of 4,500 microstrains for FRC beams; while 2,700 microstrains to 3,300 microstrains with an average of 2,950 microstrains were measured for the plain concrete beams.
5. With the addition of fibers, the flexural behavior exhibits an improved ductility index When compared to plain concrete beams, FRC beams failed in a relatively more ductile fashion.
6. With the addition of polypropylene fibers, the ductility indices increased by approximately 40% based on Jaeger approach. In addition, both plain concrete beams and FRC beams provided adequate deformability level, as described by Jaeger approach.

ACKNOWLEDGMENTS

The authors gratefully acknowledge the financial support of the Missouri Department of Transportation and UMR University Transportation Center for this joint research program. The authors are also thankful to Doug Gremel of Hughes Brothers and Don Smith of SI Concrete Systems for their participation on the Research Advisory Panel as well as the generous in-kind material donation to this project.

REFERENCES

1. Naaman, A.E., and Jeong, S.M. “Structural Ductility of Concrete Beams Prestressed with FRP Tendons,” *Proc., 2nd Int. RILEM Symp. (FRPRXS-2), Non-Metric (FRP) Reinforcement for Concrete Structures*, RILEM, Bagneux, France, 1995, pp. 379-386.

2. Jaeger, G.L., Tadros, G., and Mufti, A.A., “Balanced Section, Ductility and Deformability in Concrete with FRP Reinforcement,” *Research Report* No. 2-1995, Industry Center for Computer-Aided Engineering, Technical University of Nova Scotia, Halifax, Nova Scotia, Canada, 1995, 29 pp.

3. Belarbi, A., Chandrashkhara, K., and Watkins, S.E., "Performance Evaluation of FRP Rebar Featuring Ductility and Health Monitoring Capability," Proceedings of the Fourth International Symposium on Fiber Reinforced Polymer for Reinforced Concrete Structures (FRPRCS-4), Baltimore, MD, October 31 - November 5, 1999, pp. 1-12

4. Harris, H.G., Somboonsong, W., and Ko, F. K., "New Ductile Hybrid FRP Reinforcing Bar for Concrete Structures," *Journal of composites for construction*, Vol. 2, No. 1, February 1998, pp. 28-37.

5. ACI committee 440, "*Guide for the Design and Construction of Concrete Reinforced with FRP Bars,*" ACI 440.1R-03, American Concrete Institute, Farmington Hills, Michigan, 2003, 41 pp.

6. Alsayed, S.H., and Alhozaimy, A.M., "Ductility of Concrete Beams Reinforced with FRP Bars and Steel Fibers," *Journal of Composite Materials*, Vol. 33, No. 19, 1999, pp. 1792-1806.

7. Li, V.C., and Wang, S., "Flexural Behaviors of Glass Fiber-Reinforced Polymer (GFRP) Reinforced Engineered Cementitious Composite Beams," *ACI Materials Journal* Vol. 99, No. 1, January-February 2002, pp. 11-21.

8. Gergely, P, and Lutz, L.A., "Maximum Crack Width in Reinforced Concrete Flexural Members," *Causes, Mechanism, and Control of Cracking in Concrete*, SP-20, American Concrete Institute, Farmington Hills, Michigan, 1999, pp.87-117.

9. Toutanji, H. A. and Saafi, M., "Flexural Behavior of Concrete Beams Reinforced with Glaass Fiber-Reinforced Polymer (GFRP) Bars," *ACI Structural Journal*, Vol. 97, No. 5, September-October 2000, pp. 712-719.

10. Salib, S.R. and Abdel-Sayed, G., "Prediction of Crack Width for Fiber-Reinforced Polymer-Reinforced Concrete Beams," *ACI Structural Journal*, Vol. 101, No. 4, July-August 2004, pp. 532-536.

11. ACI Committee 318. *"Building Code Requirements for Structural Concrete (318-02) and Commentary (318R-02),"* American Concrete Institute, Farmington Hills, Michigan, 2002, 443 pp.

12. Belarbi. A and Wang, H**.,** "Bond Splitting Behavior of FRP Reinforcing Bars Embedded in Fiber Reinforced Concrete," *Proceeding for the 84th Transportation Research Board Annual Meeting, 2005*, Washington D.C.

13. Tighiouart, B. Benmokrane, B., and Gao, D., "Investigation of Bond In Concrete Member With Fiber Reinforced Polymer (FRP) Bars," *Construction and Building Materials*, Vol. 12, No. 8, December 1998, pp. 453-462.

14. CAN/CSA-S6-00, 2000, "Canadian Highway Bridge Design Code," Canadian Standard Association, Rexdale, Ontario, Canada, 190 pp.

Table 1--Flexural Beam Test Matrix

Specimen I.D.	f_c' (MPa)	A_f (mm^2)	ρ_f/ρ_{fb}	V_f (%)
P4G	48	5#4=723	3.51	0
P8G	48	2#8=1077	3.6	0
P4C	48	2#4=219	3.16	0
F4G	30	5#4=723	4.71	0.5
F8G	30	2#8=1077	4.83	0.5
F4C	30	2#4=219	4.24	0.5

Note: each testing parameter has two identical beams, total of 12 beams.

Table 2--Average Crack Spacing

Specimen I.D.	Crack Spacing, *S*, at 40%M_u (mm)	Crack Spacing, *S*, at 80%M_u (mm)	$\frac{S_{FRC}}{S_{plain}}$ at 40%M_u	$\frac{S_{FRC}}{S_{plain}}$ at 80%M_u
P4C	152	116	---	---
P4G	134	91	---	---
P8G	152	107	---	---
F4C	117	107	0.77	0.93
F4G	102	87	0.76	0.96
F8G	122	112	0.80	1.04

M_u: Ultimate Moment

Table 3--Comparison of Crack Width between Plain Concrete Beams and FRC Beams at Service Load

Specimen I.D.	P4C	P4G	P8G	F4C	F4G	F8G
Crack Width (mm)	0.60	0.49	0.45	0.54	0.41	0.36
% decrease relative to respective plain concrete	---	---	---	10%	16%	20%

Note: the values are average of two beams.

Table 4-- Comparison of Flexural Behavior between FRC Beams and Plain Concrete Beams

Spec. I.D.	Ultimate Moment (kN.m.) (2)	Ultimate Deflection (mm) (3)	Ultimate Moment (kN.m.) (4)	Ultimate Deflection (mm) (5)	$\frac{M_{FRC}}{M_{Plain}}$ (6)	$\frac{\Delta_{FRC}}{\Delta_{Plain}}$ (7)
P4C	51	30	42	26	---	---
P4G	47	26	38	24	---	---
P8G	51	24	41	22	---	---
F4C	46	29	46	29	1.09	1.13
F4G	40	30	40	30	1.06	1.27
F8G	42	23	42	23	1.02	1.05

Note: Columns (4) and (5) are the normalized values of Column (3) and (4); Columns (6) and (7) are the ratios of moment or deflection between the FRC beams to those of the plain concrete beams after normalizations.

Table 5-- Predictions of Ultimate Moment Capacities

Specimen I.D.	$M_{exp.}$ (kN.m)	M_{ACI} (kN.m) ε_{cu} =0.003	$\frac{M_{ACI}}{M_{exp.}}$	M^*_{ACI} (kN.m) ε_{cu} =0.0035	$\frac{M^*_{ACI}}{M_{exp.}}$
P4C	51	40	0.79	43	0.84
P4G	47	42	0.89	44	0.94
P8G	51	46	0.89	48	0.94
Average			**0.86**		
F4C	46	33	0.72	35	0.76
F4G	40	34	0.84	36	0.88
F8G	42	37	0.88	38	0.92
Average			**0.81**		**0.86**

Table 6-- Ductility Index by Energy Based Method

Specimen I.D.	E_{tot} (N.mm)	$E_{ela.}$ (N.mm)	μ_E	$\frac{\mu_{E-FRC}}{\mu_{E-Plain}}$
P4C	3.16	1.66	1.45	1
P4G	2.52	1.58	1.30	1
P8G	2.61	1.37	1.46	1
F4C	2.76	1.30	1.56	1.07
F4G	2.51	1.29	1.48	1.14
F8G	2.07	1.04	1.50	1.03
Average				**1.08**

Table 7-- Ductility Index by Deformation Based Method

Specimen I.D.	$M_{\varepsilon=0.001}$ (kN-m.)	$\psi_{\varepsilon=0.001}$ (10^{-5}/mm.)	M_{ult} (kN.m.)	ψ_{ult} (10^{-5}/mm)	μ_E	$\frac{\mu_{E-FRC}}{\mu_{E-Plain}}$
P4C	23.00	3.08	51.13	7.22	5.21	1
P4G	20.16	2.62	46.02	6.94	6.05	1
P8G	21.56	1.95	51.02	5.8	7.04	1
F4C	18.5	2.42	45.68	8.18	8.35	1.60
F4G	17.42	2.26	40.45	8.70	8.94	1.48
F8G	17.8	1.75	41.59	5.67	7.56	1.08
Average						**1.39**

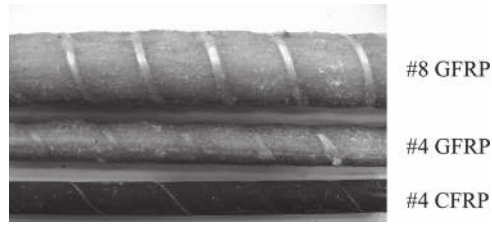

Fig. 1—Various FRP rods used in this study

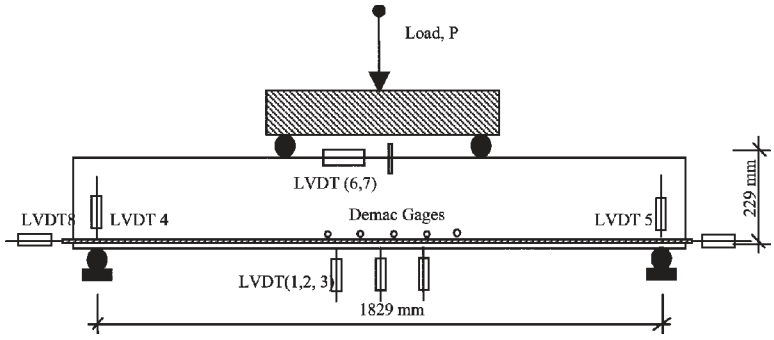

Fig. 2— Flexural Beam Test Setup

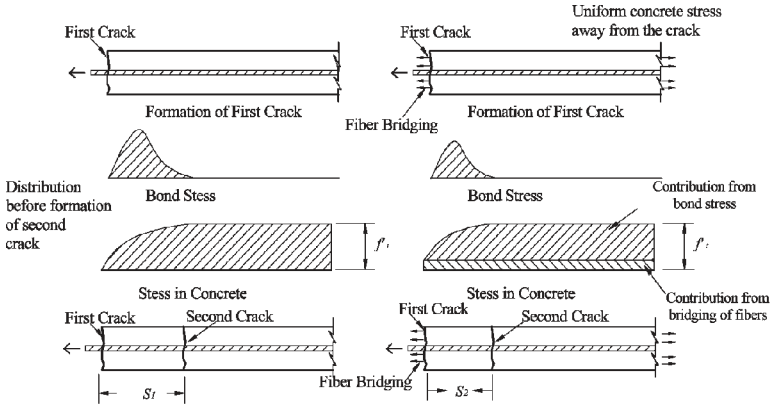

Fig. 3— Mechanism of Crack Formation in Plain Concrete and FRC

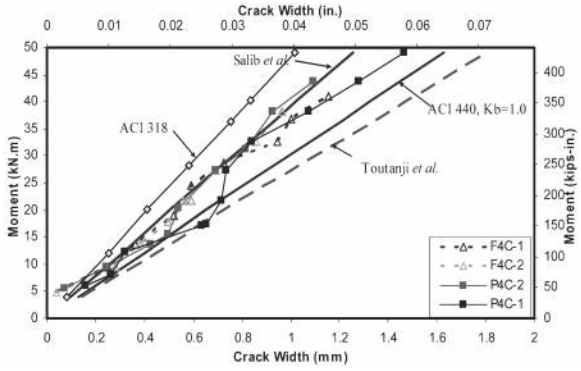

Fig. 4—Crack Width vs. Applied Moment of #4 CFRP Beams

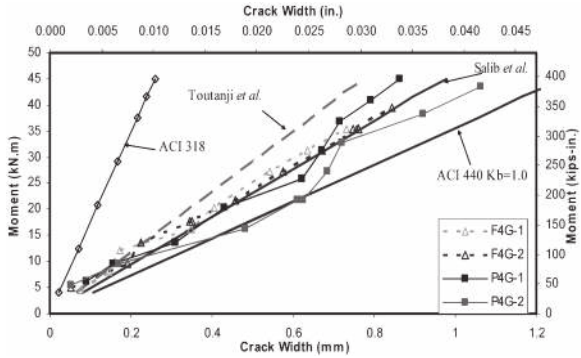

Fig. 5— Crack Width vs. Applied Moment of #4 GFRP Beams

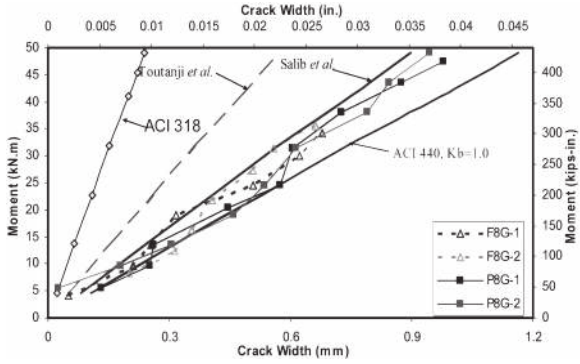

Fig. 6— Crack Width vs. Applied Moment of #8 GFRP Beams

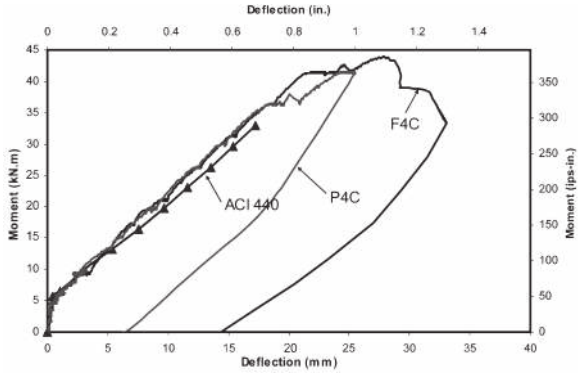

Fig. 7—Moment-Deflection Curves for #4 CFRP in Plain Concrete/FRC

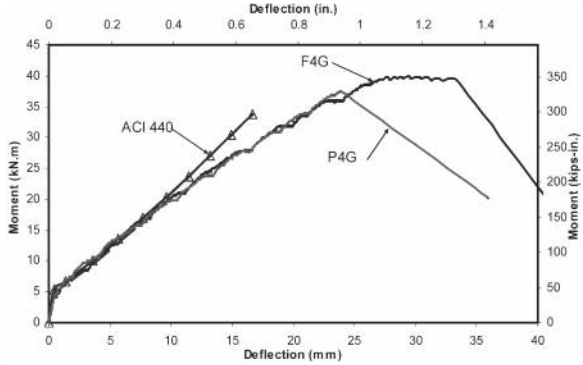

Fig. 8—Moment-Deflection Curves for #4 GFRP in Plain Concrete/FRC

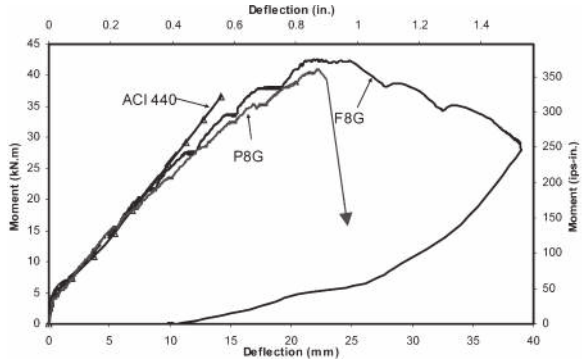

Fig. 9— Moment-Deflection Curves for #8 GFRP in Plain Concrete/FRC

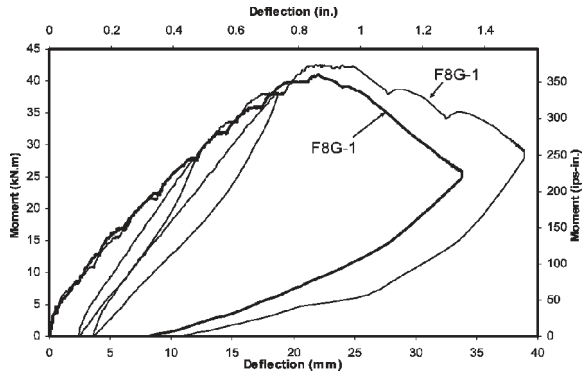

Fig. 10—Typical Loading/unloading Cycle's Effect on FRC Beams

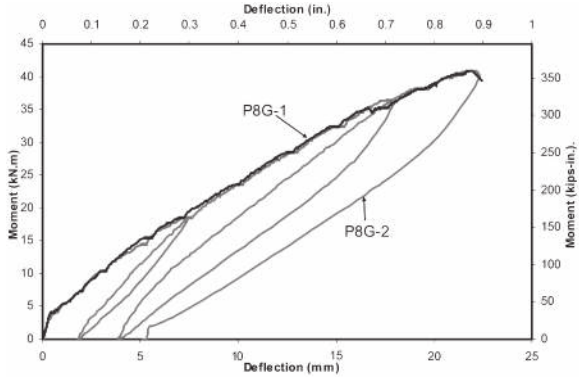

Fig. 11—Typical Loading/unloading Cycle's Effect on Plain Concrete Beams

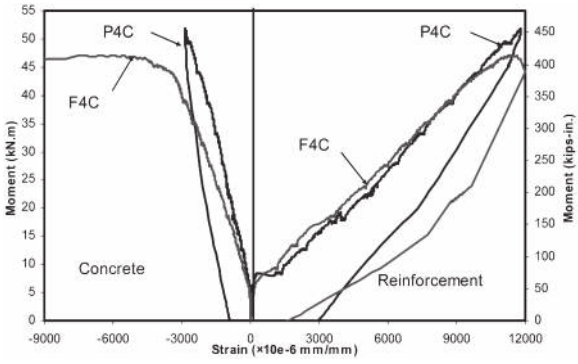

Fig. 12—Typical Strain Distributions in Reinforcement and Concrete

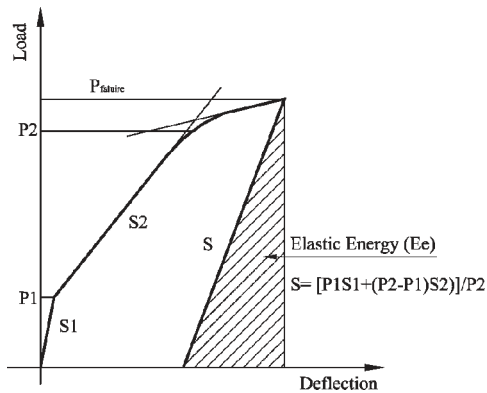

Fig. 13—Naaman and Jeong's Definition of Ductility Index

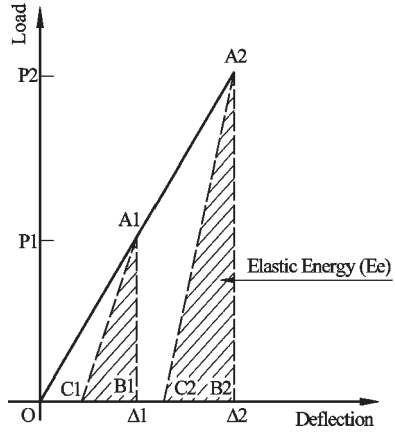

Fig. 14—Idealized Load-Deflection Curves